



# Study of spin symmetry in the doped $t$ - $J$ model using infinite projected entangled pair states

Jheng-Wei Li <sup>1</sup>, Benedikt Bruognolo,<sup>1,2</sup> Andreas Weichselbaum,<sup>3,1</sup> and Jan von Delft<sup>1</sup>

<sup>1</sup>*Arnold Sommerfeld Center for Theoretical Physics, Center for NanoScience, and Munich Center for Quantum Science and Technology, Ludwig-Maximilians-Universität München, 80333 Munich, Germany*

<sup>2</sup>*Max-Planck-Institut für Quantenoptik, Hans-Kopfermann-Strasse 1, D-85748 Garching, Germany*

<sup>3</sup>*Department of Condensed Matter Physics and Materials Science, Brookhaven National Laboratory, Upton, New York 11973-5000, USA*

 (Received 18 June 2020; revised 25 January 2021; accepted 29 January 2021; published 15 February 2021)

We study the two-dimensional  $t$ - $J$  model on a square lattice using infinite projected entangled pair states (iPEPS). At small doping, multiple orders, such as antiferromagnetic order, stripe order and superconducting order, are intertwined or compete with each other. We demonstrate the role of spin symmetry at small doping by either imposing SU(2) spin symmetry or its U(1) subgroup in the iPEPS ansatz, thereby excluding or allowing spontaneous spin-symmetry breaking, respectively, in the thermodynamic limit. From a detailed comparison of our simulations, we provide evidence that stripe order is pinned by long-range antiferromagnetic order. We also find SU(2) iPEPS, enforcing a spin-singlet state, yields a uniform charge distribution and favors  $d$ -wave singlet pairing.

DOI: [10.1103/PhysRevB.103.075127](https://doi.org/10.1103/PhysRevB.103.075127)

## I. INTRODUCTION

The discovery of high-temperature superconductivity has triggered intense research on the properties of the one-band  $t$ - $J$  model on a square lattice, which has been argued to capture essential low-energy properties of cuprate materials [1]. Despite many analytical and numerical works, full consensus regarding the competing low-energy states with different charge, spin, and superconducting orders of the  $t$ - $J$  model has not yet been reached. One category includes so-called stripe states, featuring spin-density waves and charge-density waves [2–24], where some of these states also exhibit co-existing  $d$ -wave superconducting order. Another potential candidate for the ground state of the hole-doped  $t$ - $J$  model is a superconducting state with uniform hole density [18,25,26]. Recently, Corboz *et al.* [24], using infinite projected entangled pair states (iPEPS), demonstrated the energetically extremely close competition of the uniform state and the stripe state, even for the largest accessible numerical simulations. Similar work on the Hubbard model also pointed towards a striped ground state [27–33]. Nevertheless, the underlying physical mechanism causing these intriguing ground-state properties remains elusive, and refined work in this direction is clearly necessary.

In this paper, we focus on the so-called  $\lambda 5$  stripe state, featuring spin and charge modulations with a period of  $\lambda = 5$  lattice spacings, which was previously shown to be energetically favorable near hole doping  $\delta \simeq 0.1$  at  $J/t = 0.4$  (referred to as the W5 stripe in [24]). We use iPEPS (i) to study the evolution of  $\lambda 5$  stripe order from its optimal doping  $\delta \simeq 0.1$  into the spin and charge uniform phase and (ii) to provide insight into the relation between stripes and long-range antiferromagnetic (AF) order in the thermodynamic limit.

In particular, we show that by implementing either U(1) or SU(2) spin symmetry in the iPEPS ansatz, the relevance of long-range AF order can be directly examined. Our analysis complements the finite-size scaling often used in density matrix renormalization group (DMRG) and quantum Monte Carlo (QMC) simulations, thereby addressing the question of “the fate of the magnetic correlations in the 2D limit” raised in Ref. [34]. Moreover, we show that the SU(2) iPEPS ansatz which, by construction, represents a spin-singlet state, possesses  $d$ -wave singlet pairing order. Such SU(2) iPEPS can be interpreted as a generalized resonating valence bond (RVB) state [35–39], and in this sense our finding of  $d$ -wave pairing for the SU(2) iPEPS is reminiscent of Anderson’s original RVB proposal [40–42].

## II. MODEL AND METHODS

The  $t$ - $J$  Hamiltonian is given by

$$\hat{H} = -t \sum_{\langle ij \rangle \sigma} (\tilde{c}_{i\sigma}^\dagger \tilde{c}_{j\sigma} + \text{H.c.}) + J \sum_{\langle ij \rangle} \left( \hat{\mathbf{S}}_i \cdot \hat{\mathbf{S}}_j - \frac{1}{4} \hat{n}_i \hat{n}_j \right), \quad (1)$$

with the spin operators  $\hat{\mathbf{S}}_i$ , projected fermionic operators  $\tilde{c}_{i\sigma} = \hat{c}_{i\sigma} (1 - \hat{c}_{i\bar{\sigma}}^\dagger \hat{c}_{i\bar{\sigma}})$ , spin label  $\sigma \in \{\uparrow, \downarrow\}$ , and  $\langle ij \rangle$  indexing all nearest-neighbor sites on a square lattice. To control the doping, we minimize  $\hat{H} - \mu \hat{N}$  for a specified choice of chemical potential  $\mu$  (see the Supplemental Material [62], Sec. S-II.). We set  $t = 1$  as the unit of energy and use  $J/t = 0.4$  throughout.

We use iPEPS to obtain an approximate ground state for Eq. (1). The iPEPS ground state is a tensor network state consisting of a unit cell of rank-5 tensors, i.e., tensors with five indices or legs, repeated periodically on an infinite

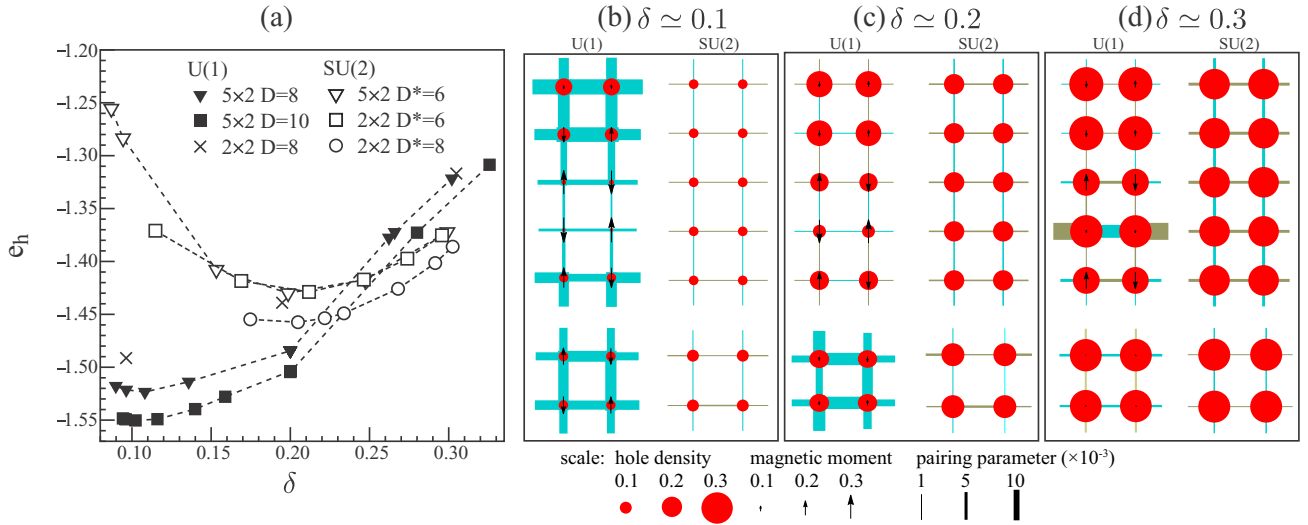


FIG. 1.  $U(1)$  and  $SU(2)$  iPEPS results for the  $t$ - $J$  model at  $J/t = 0.4$ . (a) The energy per hole  $e_h$  as a function of hole doping  $\delta$  for  $5 \times 2$  and  $2 \times 2$  unit cells. (b)–(d) Spin, hole, and singlet pairing amplitude profiles at  $\delta \approx 0.1, 0.2$ , and  $0.3$ .  $U(1)$  iPEPS ( $D = 8$ ) yields stripes on  $5 \times 2$  clusters and charge-uniform states on  $2 \times 2$  clusters;  $SU(2)$  iPEPS ( $D^* = 6$ ) yields spin singlets. Symbols and linewidths are drawn to scale as indicated.

square lattice [24,43–48]. Each rank-5 tensor has one physical index and four virtual indices (bonds) connecting to the four nearest-neighboring sites. The accuracy of such a variational ansatz is guaranteed by the area law and can be systematically improved by increasing the bond dimension  $D$ .

Using the QSPACE tensor network library [49], we can simply switch between exploiting either  $U(1)$  or  $SU(2)$  spin symmetries for our iPEPS implementation [50]. This allows us to use sufficiently large bond dimensions to obtain accurate ground state wave functions. With  $SU(2)$  iPEPS [35–39,50–55], we push the reduced bond dimension  $D^*$  up to 8, where  $D^*$  is the number of retained  $SU(2)$  multiplets per virtual bond, which corresponds to a full bond dimension of  $D \approx 13$  states. To optimize the iPEPS wave functions via imaginary-time evolution, we use full-update and fast full-update methods [24,45,47,56,57]. The contraction of the two-dimensional infinite lattice is evaluated approximately by the corner transfer matrix method [24,58–61], which generates so-called environment tensors with an environment bond dimension  $\chi$ . For  $SU(2)$  iPEPS, the environment bond dimensions used here are  $\chi^* = 144$  ( $\chi \approx 300$ ) for  $D^* = 6$  ( $D \approx 11$ ) and  $\chi^* = 128$  ( $\chi \approx 270$ ) for  $D^* = 8$  ( $D \approx 13$ ). For  $U(1)$  iPEPS, the environment bond dimensions are  $\chi = 256$  for  $D = 8$  and  $\chi = 200$  for  $D = 10$ .

### III. ENERGETICS

In Fig. 1(a), we show the energy per hole,  $e_h(\delta) \equiv (e_s - e_0)/\delta$ , as a function of hole doping  $\delta$ , obtained from various iPEPS simulations (plots of  $e_s(\delta)$  vs  $\delta$  are shown in the Supplemental Material [62], Fig. S3). Here  $e_s$  is the average ground state energy per site, and  $e_0 = -0.467775$  is the numerically exact value for the AF phase at zero doping taken from Ref. [63]. Using  $U(1)$  iPEPS on a  $5 \times 2$  unit cell, we find a minimum at  $\delta_c \approx 0.1$ , as previously reported [24]. If phase separation, involving a mixture of AF and stripe orders, sets in with decreasing  $\delta$ , then  $\delta_c$  provides an upper bound

for this onset (see the Supplemental Material for details). Increasing the bond dimension from  $D = 8$  to  $D = 10$  improves the ground state energy consistently for every doping  $\delta$  considered here. On the other hand, using  $SU(2)$  iPEPS ( $D^* = 6$ ), we obtain a spin-singlet state with no stripe feature on a  $5 \times 2$  unit cell. Moreover, the ground state energy is almost independent of the shape of unit cells (compare  $5 \times 2$  and  $2 \times 2$  data). We further improve the ground states using  $D^* = 8$  on the  $2 \times 2$  unit cell. Overall, for  $\delta \lesssim 0.2$  in Fig. 1(a), we see that the  $U(1)$   $\lambda_5$  stripe state yields a substantially lower ground state energy than the spin-singlet state, while the latter lies below the former for  $\delta \gtrsim 0.25$ . From a technical perspective, our calculations show that for the non-symmetry-breaking phase favored at  $\delta \gtrsim 0.25$ ,  $SU(2)$  iPEPS benefits from the full utilization of the spin-rotational symmetry, even though  $U(1)$  iPEPS has a larger number of variational parameters when  $D > D^*$ .

Next, we take a close look at each individual iPEPS for three values of doping. The stripe states obtained using  $U(1)$  iPEPS, shown in the top left parts of Figs. 1(b)–1(d), exhibit modulation of charge and spin densities along the  $y$  direction. At  $\delta \approx 0.1$ , we find hole doping to be maximal along the top row, implying a site-centered stripe, in agreement with previous work [24]. Note that the spins in the two rows on either side of the top row (rows 2 and 5) are ordered antiferromagnetically (implying a so-called  $\pi$  phase shift across the top row), thereby reducing the energy of transverse hole hopping along the domain wall [10,11,16]. At  $\delta \approx 0.2$ , we find hole doping to be maximal between two rows (the first and second), implying a bond-centered stripe, as frequently observed in DMRG, density matrix embedding theory (DMET), and QMC calculations [10,27]. Finally, at  $\delta \approx 0.3$ , the hole densities are roughly equal across all sites, with residual charge and spin modulation. Overall, the stripe states we find here are in agreement with previous studies, which concluded that in the  $t$ - $J$  model stripe formation is predominantly driven by the competition between the kinetic energy and the exchange

energy [2,3,9,15]. However, the same mechanism can also induce the pairing formation [12,18,26,64]. Therefore, it is *a priori* unclear under what circumstances the system will favor stripe order or pairing at small doping. To clarify this issue, we now turn to our SU(2) iPEPS results.

In contrast to the U(1) iPEPS results, switching on spin-rotational symmetry on the  $5 \times 2$  unit cell by using SU(2) iPEPS suppresses the AF order and hence the spin modulation, as shown in the top right parts of Figs. 1(b)–1(d). The resulting state no longer shows any spin stripes and instead has the same structure as the uniform state obtained on a  $2 \times 2$  unit cell at similar doping [see the bottom right parts of Figs. 1(b)–1(d)]. In addition, enforcing SU(2) symmetry also makes charge modulations completely disappear as well. This observation suggests that in the  $t$ - $J$  model charge density waves are strongly tied to spin stripes.

We have also examined  $d$ -wave superconducting order by computing the singlet pairing amplitude,  $\langle \Delta_{ij} \rangle = \frac{1}{\sqrt{2}} \langle \tilde{c}_{i\uparrow} \tilde{c}_{j\downarrow} - \tilde{c}_{i\downarrow} \tilde{c}_{j\uparrow} \rangle$ . For the U(1) iPEPS  $\lambda 5$  stripe states in Figs. 1(b)–1(d), we cannot directly identify a  $d$ -wave pairing character, in contrast to Refs. [24,27], which found opposite signs for the amplitude of the bonds along the  $x$  and  $y$  axes. However, a word of caution is necessary in reading this result when the ground state spontaneously breaks SU(2) spin symmetry because even a trivial term, such as  $\langle \tilde{c}_{i\uparrow} \tilde{c}_{j\downarrow} \rangle$ , could yield a nonzero contribution to  $\langle \Delta_{ij} \rangle$ . For a more rigorous diagnosis, one should explicitly study the pair correlation function [34,65–67], which goes beyond the scope of this work. Hence, our results do not exclude the possibility that stripes and  $d$ -wave superconducting order could coexist. For example, in the case of the U(1) results of Figs. 1(b)–1(d) we find that local  $d$ -wave order including the proper signs is absent at  $\delta \simeq 0.1$  and  $0.2$ . However, it is present for the  $2 \times 2$  U(1) cell at  $\delta \simeq 0.3$ , where the local magnetization is too small to sustain significant AF order.

On the other hand, the SU(2) iPEPS is a spin-singlet state by construction. It takes into account short-range spin correlations but excludes long-range AF order, which breaks spin-rotational symmetry in the thermodynamic limit (see the Supplemental Material for details). This rules out the aforementioned ambiguity, and the singlet pairing amplitude becomes a robust measure. As shown in Figs. 1(b)–1(d), a  $d$ -wave pattern appears on both the  $5 \times 2$  and  $2 \times 2$  unit cells. Figure 2 shows the averaged singlet pairing amplitude,  $\bar{\Delta} = \frac{1}{N} \sum_{\langle ij \rangle} f(\mathbf{r}_{ij}) \langle \Delta_{ij} \rangle$ , as a function of doping, where  $N$  is the number of sites in the unit cells,  $\mathbf{r}_{ij} \equiv \mathbf{r}_j - \mathbf{r}_i$ , and  $f(\mathbf{r})$  is a  $d$ -wave form factor, which takes the values  $f(\pm \hat{y}) = -1$  and  $f(\pm \hat{x}) = 1$ , respectively. The error bar indicates the mean absolute deviation of the pairing amplitudes among all bonds. In the  $2 \times 2$  case, the pronounced deviation is mostly attributed to the difference in pairing amplitudes along the  $x$  and  $y$  directions. A similar phenomenon was also observed in a recent large-scale DMRG calculation [34], and an almost equal mixture between  $d$ -wave and  $s$ -wave singlet pairing amplitude was suggested. Upon increasing the bond dimension  $D^*$  from 6 to 8, the  $d$ -wave pairing order increases. This is different from the previous analysis of charge uniform states using U(1) iPEPS, where pairing is suppressed with increasing  $D$  [24]. Furthermore, the  $5 \times 2$  case also shows a rather uniform  $d$ -wave pattern. The magnitude of the pairing

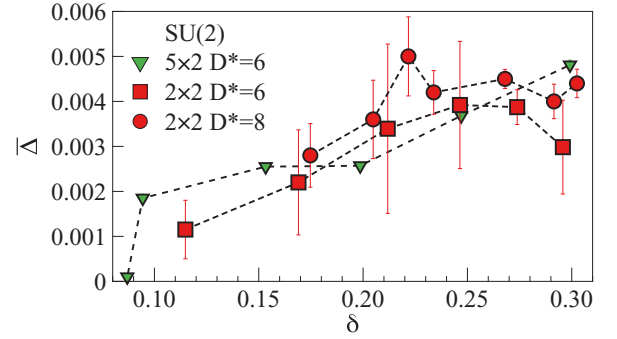


FIG. 2. Averaged singlet pairing amplitude as a function of doping using SU(2) iPEPS. The error bar shows the mean absolute deviation of the pairing amplitudes among all bonds. For the  $5 \times 2$  unit cell, the error bars are smaller than the symbols.

amplitude in Fig. 2 is small but finite, even if about an order of magnitude smaller than reported in other U(1) iPEPS or DMRG simulations [19,21,24]. This appears consistent with Fig. 1(d) for  $\delta \simeq 0.3$ , showing  $d$ -wave order with an amplitude slightly smaller for  $2 \times 2$  SU(2) than for  $2 \times 2$  U(1) or  $5 \times 2$  SU(2), which are comparable. All in all, our SU(2) iPEPS results show that, if spin rotational symmetry is enforced, the doped  $t$ - $J$  model exhibits  $d$ -wave superconductivity in the thermodynamic limit, in agreement with an early prediction from mean-field theory [41].

#### IV. INFLUENCE OF STRIPES ON ANTIFERROMAGNETIC ORDER

In the previous section we showed that stripes can be stabilized as ground states using the U(1) iPEPS at doping  $0.1 \lesssim \delta \lesssim 0.2$  on a  $5 \times 2$  unit cell. By contrast, the SU(2) iPEPS shows no signature of any spatial modulations of spin and charge density. This suggests that the stripes and the AF order are intimately related. While such a viewpoint has been discussed extensively both theoretically and experimentally since the discovery of the so-called  $\frac{1}{8}$  anomaly [68–71], direct understanding of how AF order coexists with stripes is still lacking.

To address this, we have computed the staggered spin-spin correlation functions for the ground state,

$$C(i) = \frac{(-1)^{x+y}}{\frac{3}{4}(1-\delta)N} \sum_{j \in \text{unit cell}} \langle \hat{S}_{j+i} \cdot \hat{S}_j \rangle, \quad (2)$$

with  $i = (x, y)$ . The prefactor normalizes the same-site correlator to unity,  $C(0) = 1$ , given  $(1-\delta)N$  spins per unit cell. This facilitates the comparison of different unit cells and doping. In the following, we analyze  $C(i)$  along the long ( $y$ ) and short ( $x$ ) directions of the unit cell.

First, we study the staggered spin-spin correlations on a  $5 \times 2$  unit cell at doping  $\delta \simeq 0.1, 0.2$ , and  $0.3$ , using U(1) iPEPS. In Fig. 3(a), we can clearly identify  $\lambda 5$  stripe order at  $\delta \simeq 0.1$  and  $0.2$ , with staggered spin-spin correlations oscillating around zero, reflecting the pattern already seen in the left panels of Figs. 1(b) and 1(c). The staggered magnetic order undergoes a phase shift of  $\pi$  across the length of the  $5 \times 2$  unit cell, resulting in a period of  $\lambda_m = 10$ . At doping  $\delta \simeq 0.3$ , the correlations decay much more rapidly, with weak residual

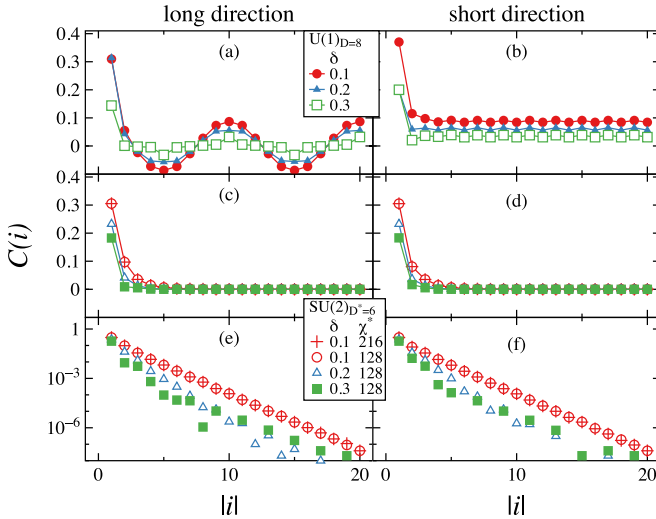


FIG. 3. Normalized staggered spin-spin correlation functions, computed on a  $5 \times 2$  unit cell along the long ( $y$ ) direction (left column) and the short ( $x$ ) direction (right column), using (a) and (b) U(1) iPEPS and (c)–(f) SU(2) iPEPS, on linear and semilogarithmic scales, respectively. Solid symbols indicate the variational state [U(1) or SU(2)] with the lower energy for a given  $\delta$ .

oscillations remaining at large distances. Given its higher variational energy compared to its SU(2) counterpart, this reflects the numerical inefficiency of using a broken-symmetry ansatz to simulate a spin singlet when many low-energy states are nearly degenerate. By contrast, Fig. 3(b) shows that the correlations along the “short” direction decrease with doping but remain positive at large distances, indicating long-range AF order, i.e.,  $C(|i| \rightarrow \infty) \neq 0$ , although attenuated with increasing  $\delta$ . Therefore, Figs. 3(a) and 3(b) suggest that stripes along the long direction go hand in hand with long-range AF order along the short direction.

To further elucidate this point, we turn our attention to the SU(2) iPEPS. Again, we have computed the staggered spin-spin correlations on a  $5 \times 2$  unit cell using SU(2) iPEPS. In Figs. 3(c) and 3(d), the correlations along the long and short directions are nearly identical and rapidly decay to zero, showing no sign of either stripes or the long-range AF order. Note that for SU(2) iPEPS, the instability of a given state towards AF order can be detected by the increase in correlation length with increasing  $\chi^*$ . (We illustrate this for the Heisenberg model in the Supplemental Material [62], Sec. SI). However, this tendency is not observed at  $\delta = 0.1$  [see Figs. 3(e) and 3(f)]. In short, we conclude that stripes emerge only in the presence of long-range AF order.

To strengthen our previous statement, we further consider  $L \times 2$  unit cells with  $L = 5, 4, 3, 2$  at  $\delta \simeq 0.2$  using U(1) iPEPS ( $D = 8$ ). Those could host spin stripes of periods  $\lambda = L$  or an AF ordered state for  $L = 2$ . A previous iPEPS study showed a very close competition between a  $\lambda 5$  stripe state and an AF state with uniform charge distribution ( $L = 2$ ) at  $\delta \simeq 0.1$  [24]. For a  $2 \times 2$  unit cell [Fig. 4(a)], the spin-spin correlations along both the long and short directions quickly decay to nearly zero, showing that AF order is weak at  $\delta \simeq 0.2$  if a charge-uniform state is assumed. The same charge-uniform state is also favored for a  $4 \times 2$  unit cell:

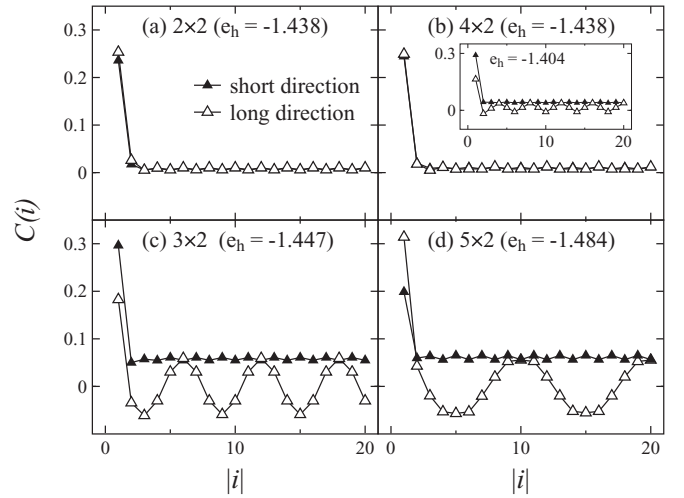


FIG. 4. Comparison of normalized staggered spin-spin correlation functions for  $\delta \simeq 0.2$  using U(1) iPEPS at  $D = 8$  along the long ( $y$ ) direction and the short ( $x$ ) direction on  $L \times 2$  unit cells for  $L = 2, 3, 4, 5$  in (a)–(d), respectively. The inset in (b) is a  $\lambda 4$  stripe state obtained from different initialization.

we obtain this by initializing the  $4 \times 2$  unit cell of a full-update optimization using two copies of the  $2 \times 2$  unit cell in Fig. 4(a), which yields a slightly lower energy than a  $\lambda 4$  stripe state [inset in Fig. 4(b)] initialized from simple-update results. By contrast,  $3 \times 2$  and  $5 \times 2$  unit cells show a clear stripe feature along the long direction, together with nonzero long-range AF order along the short one [Figs. 4(c) and 4(d)], and slightly lower ground state energy than those of  $2 \times 2$  and  $4 \times 2$ . However, the bond dimension  $D$  used here is not large enough to conclusively resolve the close competition between the different states. Overall, by plotting the correlations along both the short and long directions in the same panel, we see that the amplitude of the stripe modulation is the same as that of attenuated long-range AF correlations. This further confirms that the stripes and the long-range AF order are indeed tied to each other at finite doping.

## V. SUMMARY

We have studied the doped  $t$ - $J$  model with  $J/t = 0.4$  using U(1) and SU(2) iPEPS. For doping  $0.1 \lesssim \delta \lesssim 0.2$ , the  $\lambda 5$  striped charge and spin order with U(1) symmetry is energetically favorable compared to a spin-singlet state with SU(2) symmetry. By contrast, for  $\delta \gtrsim 0.25$ , the latter is favored. By studying the spin-spin correlations, we find a close link between stripe order and long-range AF order. At small doping, the U(1) iPEPS shows that spin stripes emerge along one spatial direction, while attenuated long-range AF order persists along the other spatial direction. Upon increasing doping, the strength of stripe order decreases hand in hand with long-range AF order. By contrast, the SU(2) iPEPS, which does not break spin rotational symmetry, excludes long-range AF order and hence stripe formation but yields  $d$ -wave superconducting order at finite doping. Our study demonstrates the utility and importance of being able to turn on and off the SU(2) spin-rotational symmetry at will—it gives direct insight



into the interplay between regimes with spontaneously broken symmetries and where  $SU(2)$  invariance remains intact.

### ACKNOWLEDGMENTS

The Deutsche Forschungsgemeinschaft supported B.B., J.-W.L., and J.v.D. through the Excellence Cluster

“Nanosystems Initiative Munich” and the Excellence Strategy-EXC-2111-390814868. J.-W.L. was also supported by German Research Foundation (DFG WE4819/3-1) under Germany’s Excellence Strategy—EXC-2111-390814868. A.W. was supported by the U.S. Department of Energy, Office of Basic Energy Sciences, under Contract No. DE-SC0012704.

- 
- [1] F. C. Zhang and T. M. Rice, *Phys. Rev. B* **37**, 3759 (1988).  
 [2] D. Poilblanc and T. M. Rice, *Phys. Rev. B* **39**, 9749 (1989).  
 [3] J. Zaanen and O. Gunnarsson, *Phys. Rev. B* **40**, 7391 (1989).  
 [4] K. Machida, *Physica C (Amsterdam, Neth.)* **158**, 192 (1989).  
 [5] H. Schulz, *J. Phys. (Paris)* **50**, 2833 (1989).  
 [6] S. R. White, D. J. Scalapino, R. L. Sugar, N. E. Bickers, and R. T. Scalettar, *Phys. Rev. B* **39**, 839 (1989).  
 [7] V. J. Emery, S. A. Kivelson, and H. Q. Lin, *Phys. Rev. Lett.* **64**, 475 (1990).  
 [8] V. Emery and S. Kivelson, *Physica C (Amsterdam, Neth.)* **209**, 597 (1993).  
 [9] C. Nayak and F. Wilczek, *Phys. Rev. Lett.* **78**, 2465 (1997).  
 [10] S. R. White and D. J. Scalapino, *Phys. Rev. Lett.* **80**, 1272 (1998).  
 [11] S. R. White and D. J. Scalapino, *Phys. Rev. Lett.* **81**, 3227 (1998).  
 [12] S. R. White and D. J. Scalapino, *Phys. Rev. B* **60**, R753(R) (1999).  
 [13] H. Eskes, O. Y. Osman, R. Grimberg, W. van Saarloos, and J. Zaanen, *Phys. Rev. B* **58**, 6963 (1998).  
 [14] L. P. Pryadko, S. A. Kivelson, V. J. Emery, Y. B. Bazaliy, and E. A. Demler, *Phys. Rev. B* **60**, 7541 (1999).  
 [15] S. R. White and D. J. Scalapino, *Phys. Rev. B* **61**, 6320 (2000).  
 [16] A. L. Chernyshev, S. R. White, and A. H. Castro Neto, *Phys. Rev. B* **65**, 214527 (2002).  
 [17] A. Himeda, T. Kato, and M. Ogata, *Phys. Rev. Lett.* **88**, 117001 (2002).  
 [18] C.-P. Chou, N. Fukushima, and T. K. Lee, *Phys. Rev. B* **78**, 134530 (2008).  
 [19] S. R. White and D. J. Scalapino, *Phys. Rev. B* **79**, 220504(R) (2009).  
 [20] K.-Y. Yang, W. Q. Chen, T. M. Rice, M. Sigrist, and F.-C. Zhang, *New J. Phys.* **11**, 055053 (2009).  
 [21] P. Corboz, S. R. White, G. Vidal, and M. Troyer, *Phys. Rev. B* **84**, 041108(R) (2011).  
 [22] S. Sorella, G. B. Martins, F. Becca, C. Gazza, L. Capriotti, A. Parola, and E. Dagotto, *Phys. Rev. Lett.* **88**, 117002 (2002).  
 [23] W.-J. Hu, F. Becca, and S. Sorella, *Phys. Rev. B* **85**, 081110(R) (2012).  
 [24] P. Corboz, T. M. Rice, and M. Troyer, *Phys. Rev. Lett.* **113**, 046402 (2014).  
 [25] C. S. Hellberg and E. Manousakis, *Phys. Rev. Lett.* **83**, 132 (1999).  
 [26] M. Raczkowski, M. Capello, D. Poilblanc, R. Frésard, and A. M. Oleś, *Phys. Rev. B* **76**, 140505(R) (2007).  
 [27] B.-X. Zheng, C.-M. Chung, P. Corboz, G. Ehlers, M.-P. Qin, R. M. Noack, H. Shi, S. R. White, S. Zhang, and G. K.-L. Chan, *Science* **358**, 1155 (2017).  
 [28] E. W. Huang, C. B. Mendl, H.-C. Jiang, B. Moritz, and T. P. Devereaux, *npj Quantum Mater.* **3**, 22 (2018).  
 [29] K. Ido, T. Ohgoe, and M. Imada, *Phys. Rev. B* **97**, 045138 (2018).  
 [30] A. S. Darmawan, Y. Nomura, Y. Yamaji, and M. Imada, *Phys. Rev. B* **98**, 205132 (2018).  
 [31] H.-C. Jiang and T. P. Devereaux, *Science* **365**, 1424 (2019).  
 [32] B. Ponsioen, S. S. Chung, and P. Corboz, *Phys. Rev. B* **100**, 195141 (2019).  
 [33] M. Qin, C.-M. Chung, H. Shi, E. Vitali, C. Hubig, U. Schollwöck, S. R. White, and S. Zhang, *Phys. Rev. X* **10**, 031016 (2020).  
 [34] H.-C. Jiang, Z.-Y. Weng, and S. A. Kivelson, *Phys. Rev. B* **98**, 140505(R) (2018).  
 [35] D. Poilblanc, N. Schuch, D. Pérez-García, and J. I. Cirac, *Phys. Rev. B* **86**, 014404 (2012).  
 [36] L. Wang, D. Poilblanc, Z.-C. Gu, X.-G. Wen, and F. Verstraete, *Phys. Rev. Lett.* **111**, 037202 (2013).  
 [37] D. Poilblanc, P. Corboz, N. Schuch, and J. I. Cirac, *Phys. Rev. B* **89**, 241106(R) (2014).  
 [38] D. Poilblanc and M. Mambrini, *Phys. Rev. B* **96**, 014414 (2017).  
 [39] J.-Y. Chen and D. Poilblanc, *Phys. Rev. B* **97**, 161107(R) (2018).  
 [40] P. W. Anderson, G. Baskaran, Z. Zou, and T. Hsu, *Phys. Rev. Lett.* **58**, 2790 (1987).  
 [41] G. Kotliar, *Phys. Rev. B* **37**, 3664 (1988).  
 [42] P. W. Anderson, *Science* **316**, 1705 (2007).  
 [43] F. Verstraete and J. I. Cirac, *arXiv:cond-mat/0407066*.  
 [44] F. Verstraete, M. M. Wolf, D. Perez-Garcia, and J. I. Cirac, *Phys. Rev. Lett.* **96**, 220601 (2006).  
 [45] J. Jordan, R. Orús, G. Vidal, F. Verstraete, and J. I. Cirac, *Phys. Rev. Lett.* **101**, 250602 (2008).  
 [46] C. V. Kraus, N. Schuch, F. Verstraete, and J. I. Cirac, *Phys. Rev. A* **81**, 052338 (2010).  
 [47] P. Corboz, R. Orús, B. Bauer, and G. Vidal, *Phys. Rev. B* **81**, 165104 (2010).  
 [48] B. Bauer, P. Corboz, R. Orús, and M. Troyer, *Phys. Rev. B* **83**, 125106 (2011).  
 [49] A. Weichselbaum, *Ann. Phys. (NY)* **327**, 2972 (2012).  
 [50] B. Bruognolo, J.-W. Li, J. von Delft, and A. Weichselbaum, *arXiv:2006.08289*.  
 [51] S. Singh and G. Vidal, *Phys. Rev. B* **86**, 195114 (2012).  
 [52] T. Liu, W. Li, A. Weichselbaum, J. von Delft, and G. Su, *Phys. Rev. B* **91**, 060403(R) (2015).  
 [53] P. Schmoll, S. Singh, M. Rizzi, and R. Orús, *Ann. Phys. (NY)* **419**, 168232 (2020).  
 [54] C. Hubig, *SciPost Phys.* **5**, 47 (2018).  
 [55] P. Schmoll and R. Orús, *Phys. Rev. B* **102**, 241101(R) (2020).

- [56] Z. Y. Xie, H. C. Jiang, Q. N. Chen, Z. Y. Weng, and T. Xiang, *Phys. Rev. Lett.* **103**, 160601 (2009).
- [57] H. N. Phien, J. A. Bengua, H. D. Tuan, P. Corboz, and R. Orús, *Phys. Rev. B* **92**, 035142 (2015).
- [58] R. J. Baxter, *J. Stat. Phys.* **19**, 461 (1978).
- [59] T. Nishino, K. Okunishi, and M. Kikuchi, *Phys. Lett. A* **213**, 69 (1996).
- [60] T. Nishino and K. Okunishi, *J. Phys. Soc. Jpn.* **65**, 891 (1996).
- [61] R. Orús and G. Vidal, *Phys. Rev. B* **80**, 094403 (2009).
- [62] See Supplemental Material at <http://link.aps.org/supplemental/10.1103/PhysRevB.103.075127> for discussions of the 2D Heisenberg model, phase separation, d-wave order, symmetries, and some further results of our computations.
- [63] A. W. Sandvik, *Phys. Rev. B* **56**, 11678 (1997).
- [64] S. R. White and D. J. Scalapino, [arXiv:cond-mat/0006071](https://arxiv.org/abs/cond-mat/0006071).
- [65] E. Dagotto, A. Moreo, F. Ortolani, D. Poilblanc, and J. Riera, *Phys. Rev. B* **45**, 10741 (1992).
- [66] E. Dagotto, J. Riera, Y. C. Chen, A. Moreo, A. Nazarenko, F. Alcaraz, and F. Ortolani, *Phys. Rev. B* **49**, 3548 (1994).
- [67] C. Cheng, R. Mondaini, and M. Rigol, *Phys. Rev. B* **98**, 121112(R) (2018).
- [68] J. M. Tranquada, B. J. Sternlieb, J. D. Axe, Y. Nakamura, and S. Uchida, *Nature (London)* **375**, 561 (1995).
- [69] S. A. Kivelson, I. P. Bindloss, E. Fradkin, V. Oganesyan, J. M. Tranquada, A. Kapitulnik, and C. Howald, *Rev. Mod. Phys.* **75**, 1201 (2003).
- [70] M. Vojta, *Adv. Phys.* **58**, 699 (2009).
- [71] N. J. Robinson, P. D. Johnson, T. M. Rice, and A. M. Tsvelik, *Rep. Prog. Phys.* **82**, 126501 (2019).